ACS OMEGA

http://pubs.acs.org/journal/acsodf

Article

Piezoresistive Behavior of Polypyrrole:Carboxymethyl Cellulose Composites

Van At Nguyen, Mariam Odetallah, Gorkem Bakir, Kathleen Gough, and Christian Kuss*

Cite This: *ACS Omega* 2022, 7, 41937−41942

Read Online

ACCESS | Metrics & More | Article Recommendations

ABSTRACT: The unique properties of conducting polymers make them ideally suited for applications in organic electronics, photovoltaics, and energy storage systems. Depending on the specific application, they can outperform metal-based electronics by cost, mechanical flexibility, molecular design opportunities, and environmental impact. Many composites of conducting polymers with polyanions can be processed in water. However, the facile processing of such composites comes at a cost of reduced conductivity. In this manuscript, electronic conductivity dependence on composition for a composite of polypyrrole (PPy) with carboxymethyl cellulose (CMC) has been studied. Secondary ion mass spectrometry and electron energy loss spectroscopy mapping indicate the formation of a nanostructure forming PPy-rich nanospheres with a CMC-rich surface coverage. This structure requires inter-particle electron conduction to occur *via* quantum tunneling. Variations in the tunneling distance are dependent on the applied pressure, giving rise to a pressure-dependent electronic conductivity and thus piezoresistance. This behavior opens new applications of conducting polymer composites in pressure-sensitive electronic devices, providing metal-free alternatives to quantum tunneling composites.

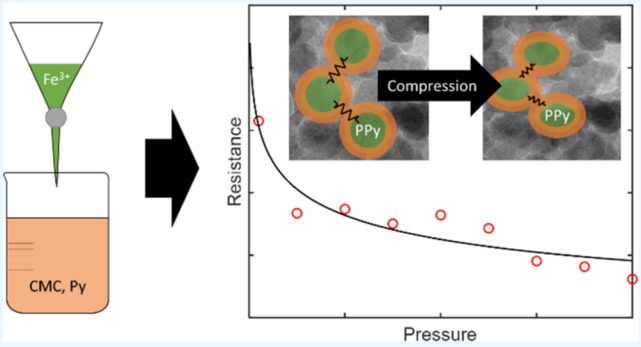

INTRODUCTION

Intrinsically conducting polymers exhibit electronic conduction, thanks to an extended conjugated bonding network along the backbone of the polymer.[1] They have found applications in organic electronics,[2] including in organic light-emitting diodes,[3] bioelectronics,[4] solar cells,[5,6] energy storage devices,[7,8] and others.[9] In many commercial applications, their processing is challenging and limits the choice of materials that can be used. In particular, the most basic conducting polymers by themselves, polyacetylene, polypyrrole (PPy), polyaniline, and polythiophene cannot be dispersed in any solvent,[9] nor can they be melted without decomposition.[10] Moreover, these polymers exhibit limited elasticity and fail easily under mechanical stress.[10] For this reason, the polymer blend of poly(3,4-ethylenedioxythiophene):poly(styrenesulfonate) (PEDOT:PSS) has found tremendous commercial success.[6,10] Ionic interactions between the positively charged backbone of PEDOT with negatively charged sulfonate groups on PSS form an irreversibly mixed composite. Due to the hydrophilicity of sulfonate groups, the composite is easily dispersed in water, notwithstanding the intrinsically hydrophobic extended conjugated bonding in the conducting polymer. The thus-formed dispersion can be processed to form coatings and bulk materials. Moreover, the composite gains elasticity from the incorporation of PSS. Consequently, the development of applications of conducting polymers has largely centered around the modification of PEDOT:PSS blends.[10]

For many large-scale applications, however, lower cost alternatives to PEDOT:PSS are required. For example, composites of PPy and cellulosic materials, including carboxymethyl cellulose (CMC), have found applications as flexible conductors, supercapacitor electrode materials,[11,12] battery electrode binders,[8,13] microbial fuel cell anodes,[14,15] and self-healing conductive hydrogels.[16] Composites of cellulosic materials have in recent years been explored in a wide range of applications for more sustainable materials toward water remediation,[17] antimicrobial fabrics,[18,19] proton conducting membranes,[20,21] and many other applications. While electrochemical pyrrole polymerization in solutions containing cellulose derivatives showed higher conductivity, chemical polymerization leads to composites that can be produced at a large scale, which are easily processed and exhibit better mechanical properties.[22] However, these

Received: June 2, 2022
Accepted: October 26, 2022
Published: November 9, 2022

composites show a rapid drop in conductivity with decreasing PPy volume fraction. For many applications of PPy:CMC, these low conductivities necessitate the addition of other conductive components, such as graphene or carbon. Few studies addressed the origin of the drastic conductivity dependence of such composites on PPy volume fraction. In PEDOT:PSS, Lang *et al.* determined the nanostructure by electron microscopy and energy-dispersive X-ray spectroscopy.[23] The authors found a core−shell nanostructure that exhibits a PEDOT-rich core and a PSS-rich surface. Horii *et al.* expanded on this work by showing that the material's hierarchical structure and primary particle size can be affected by changing the PSS content.[24] Sasso's investigation of composites of PPy with CMC, PSS, and lignosulfonate exposes ζ-potentials in composite dispersion that indicate the likely formation of composite particles exhibiting a polyanion shell.[25] Such nanostructures provide a possible explanation for the observed conductivity loss.

The current paper presents an investigation of conductivity and nanostructure of PPy:CMC composites obtained from simple, aqueous solutions. Electron microscopy and secondary ion mass spectrometry (SIMS) confirm the formation of spherical PPy-rich nanoparticles with an inhomogeneous CMC shell. An analysis of conduction behavior indicates partial control of conductivity by quantum tunneling between PPy-rich domains. For the first time, we show evidence from impedance spectroscopy that this conduction mechanism results in the piezoresistive behavior of the composite that may be exploited in pressure-sensitive electronics. Consequently, these materials represent metal-free alternatives to current commercial quantum-tunneling-based piezoresistive materials. In particular, quantum tunneling composites (QTCs) are useful for wearable, flexible electronics but limited in their applications with direct skin contact due to nickel allergies.[26] While PPy−cellulose-based composites with piezoresistive behavior have been demonstrated previously,[27] those composites require a complex microstructure design. The piezoresistance of PPy:CMC bulk materials studied here can provide a simpler and cheaper path toward metal-free flexible pressure sensors.

RESULTS AND DISCUSSION

PPy has been synthesized by oxidative chemical polymerization with ferric chloride in an aqueous solution containing CMC. The reaction yields a dark dispersion that is stable up to 1 h. Conversely, polymerization of pyrrole in water without CMC yields PPy powder that settles immediately. The composite can be separated from the solution by addition of an equal amount of ethanol to the reaction solution. After washing in ethanol and drying, electron microscopy was performed on the composite, revealing a homogeneous composite with a spherical nanostructure (Figure 1). The observed nanospheres exhibit an average diameter of 57.0 nm with a standard deviation of 5.5 nm (N = 26).

Chemical composition and microscale homogeneity were confirmed by Fourier transform infrared - attenuated total reflectance (FTIR-ATR) microscopy. Figure 2 shows the spectra of PPy and CMC separately as well as a spectrum of the composite. Chemical uniformity was assessed by processing the PPy:CMC FTIR-ATR images for the ratio of the CMC signature band at 1326 cm^{-1} to that of PPy at 963 cm^{-1}. The FTIR-ATR surface scan, rendered as a false-color image, confirms that both polymers are homogeneously

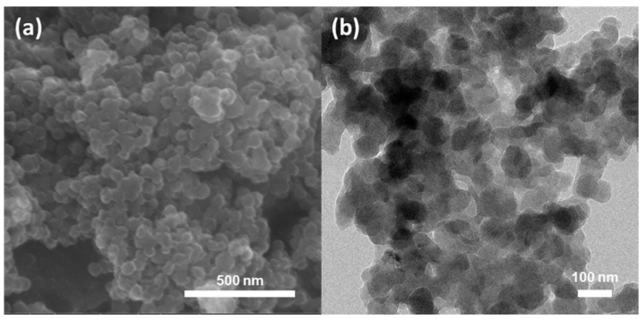

Figure 1. (a) Scanning electron microscopy (SEM) and (b) transmission electron microscopy (TEM) images of the PPy:CMC 1:1 (w/w) composite.

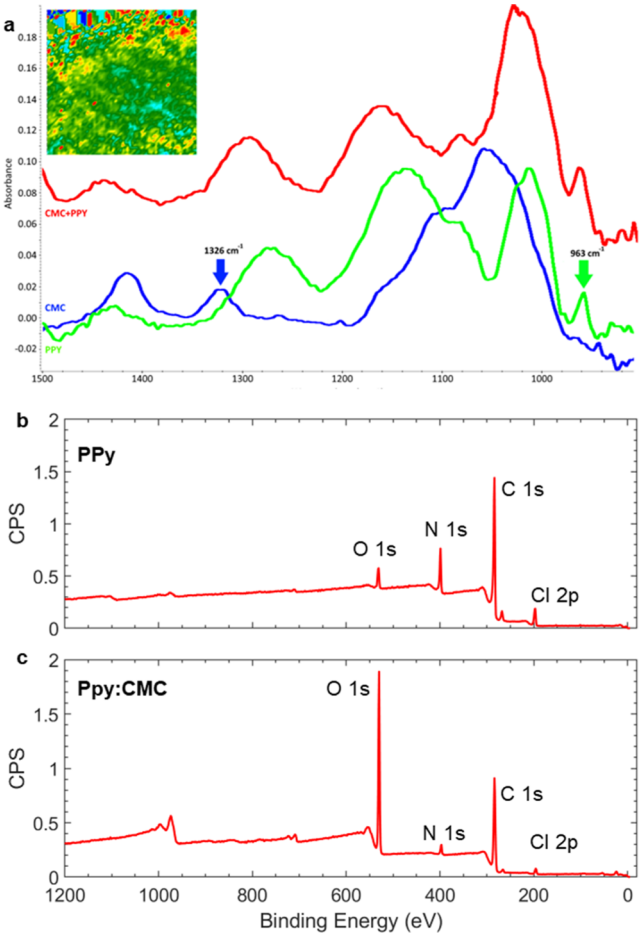

Figure 2. (a) Characteristic FTIR-ATR spectra from CMC (blue) and PPy (green) are identifiable as common features in the spectrum of PPy:CMC composite (red). The false color image of the composite, top left, was created as the ratio of characteristic bands for CMC and PPy at 1326 and 963 cm^{-1}, respectively. The color variation within the image is principally due to variable contact with the pellets. The top edge of the image shows typical peak ratio variations when the ATR probe is lacking good contact with the sample. Survey XPS spectra for PPy (b) and PPy:CMC (c) show expected elemental composition and significant attenuation of the N 1s signal after introduction of CMC. Peaks above 600 eV are assigned to iron contamination and Auger emissions from oxygen.

distributed at the microscale. Further chemical characterization by X-ray photoelectron spectroscopy is shown in Figure 2b,c, confirming the presence of all relevant elements, together with

https://doi.org/10.1021/acsomega.2c03461
ACS Omega 2022, 7, 41937−41942

a significant increase in oxygen and depletion of nitrogen at the material surface upon doping with CMC.

Measuring the electronic conductivity of the synthesized materials by a four-point probe, it is apparent that the formed PPy exhibits near-metallic conductivity around 10 S cm^{-1}. Upon addition of CMC, the composite conductivity decreases drastically (Figure 3, black circles). In a 1:1 weight ratio

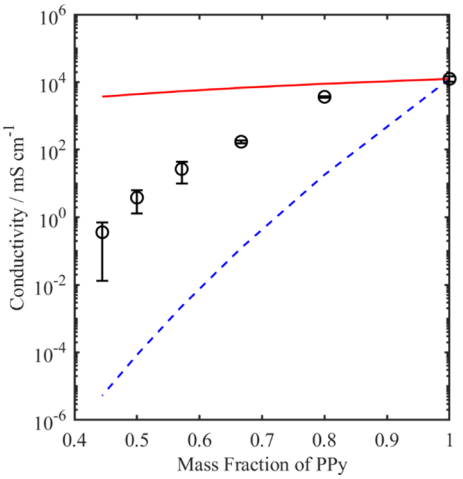

Figure 3. Trend in the electrical conductivity of PPy:CMC composites (black circles) with standard deviation and comparison to the Bruggeman relationship for spherical conductive particles in a non-conductive matrix (red solid line) and quantum tunneling conduction based on the core−shell PPy:CMC composite with full-phase separation (blue dashed line).

composite of PPy and CMC, the conductivity is reduced by a factor of more than 1000 to just below 10 mS cm^{-1}. This severe drop in conductivity affects the applicability of PPy:CMC-type conducting polymer composites. For many applications, sufficient mechanical strength of the composites is achieved at CMC weight fractions above 40%.[13]

As a composite between a conductive and a non-conductive material is formed, the effective medium approximation may be applied to estimate the apparent conductivity of the composite. The Bruggeman relationship accounts for volume fraction and path length (tortuosity) of conduction and is typically used for this purpose. It describes conductivity as an exponential function of volume fraction and is thus consistent with the observed exponential decrease in conductivity. In a conductive material with spherical, non-conductive, randomly distributed inclusions, the following relationship between apparent conductivity σ_{eff}, volume fraction ϵ, and intrinsic conductive phase conductivity σ is found[28,29]

$$\sigma_{eff} = \sigma \cdot \epsilon^{3/2} \quad (1)$$

Assuming similar densities of the two polymers, this relationship leads to a change of conductivity by less than 1 order of magnitude over the measured composition range (Figure 3, red curve). It should be noted that other disordered distributions of conducting and non-conducting material in a composite lead to a similar behavior with slight variations in the Bruggeman exponent.[30] The observed discrepancy of the slope of the conductivity with weight fraction poses a significant deviation from the expected behavior in a disordered composite. Hence, a random orientation cannot be assumed.

Instead, the composite consists of an ordered arrangement of more and less conductive areas in the material. Given previous ζ-potential measurements of PPy:CMC composites, a core−shell structure is most likely.[25] Assuming full separation of PPy and CMC, the material would exhibit a pure PPy core and a pure CMC shell, and conduction would have to occur by electron quantum tunneling. As the quantum tunneling current decreases exponentially with distance, and the thickness of the CMC layer increases near-linearly with CMC weight fraction, the observed exponential decrease in conductivity is also consistent with quantum tunneling.

Pressure-sensing materials, named QTCs, have been built based on similar structures.[31] These materials consist of metallic microparticles in an elastomeric matrix. Conduction occurs upon tunneling and is minimal in the unstrained material. Under compressive strain, the elastomeric matrix is compressed, distances between particles are reduced, and quantum tunneling conduction is drastically increased. Commercial strain sensors have been developed from these QTCs in the form of rubber mats, foams, grains, inks, and pads.[32] The here prepared conducting polymer composite material exhibits a similar behavior. We measured the impedance of PPy:CMC composite pellets between two stainless steel electrodes. The pressure between the two electrodes was controlled. Stassi *et al.* studied the impedance response of QTCs to changing pressure.[33] Their work proposed an equivalent circuit as shown in Figure 4a. The series resistor (R_s) represents intrinsic material resistances. Charge-transfer resistance (R_p) and constant phase element (CPE) in parallel represent resistance to electron tunneling between conducting particles and conductive particle surface capacitance, respectively. A CPE is used in place of a capacitor to account for a dispersion in particle size and non-conductive film thickness, as well as a non-ideal capacitive behavior. However, in all cases, the CPE's exponent β is above 0.8, approaching an ideal capacitor behavior.

Figure 4b shows that the application of pressure to PPy:CMC significantly increases its conductivity, similar to the behavior of typical QTCs. At the same time, increased pressure increases the determined capacitance, as the distance between conductive particles is reduced. As such, the impedance behavior shows both characteristic behaviors of QTCs. As typical for QTCs, this behavior is reversible (Figure 4c), showing that high resistance is recoverable upon release of pressure over multiple cycles. The conductivity in the prepared PPy:CMC composite changes by a factor of 2 within the first bar of applied pressure, which is less sensitive than typical QTCs, which apply spiky metal particles with large localized electric fields, and exhibit double the sensitivity in a sample of similar shape.[33] Yet, the conductivity behavior of PPy:CMC is clearly mirroring typical QTCs, suggesting that electron tunneling contributes to electron conduction in the produced PPy:CMC composite.

Quantum tunneling conduction exhibits a characteristic tunneling distance dependence. Electron tunneling conductivity σ_t can be expressed as a function of a constant A, the electron mass m_e, the material's work function Φ, Planck's constant h, and the tunneling distance d[34]

$$\sigma_t = A \cdot e^{\sqrt{2m_e\Phi}/hd} \quad (2)$$

It is possible to estimate the expected conductivity dependence on mass fraction for the synthesized material.

https://doi.org/10.1021/acsomega.2c03461
ACS Omega 2022, 7, 41937−41942

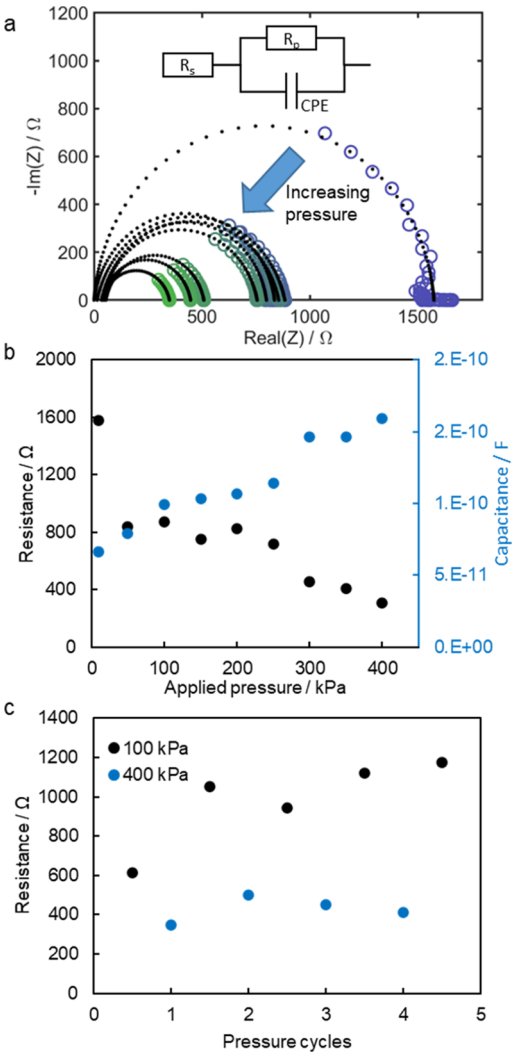

Figure 4. (a) Impedance spectra and fit for PPy:CMC pellets under varying pressure from 50 kPa (blue) to 400 kPa (green) and fitted model (black dots) with equivalent circuit;[33] (b) changes in resistance (black) and capacitance (blue) showing a strong decrease in resistance and increase of capacitance with increasing pressure; and (c) pressure cycling showing that resistance values recover reversibly after application and release of pressure.

Assuming a work function of PPy around 5 eV,[35] and similar densities of PPy and CMC, conductivity should change by 3 orders of magnitude for each 10 wt % change in mass fraction around the 1:1 ratio (Figure 3, blue curve). The observed resistance exhibits a much smaller slope. Rather, it behaves intermediate to quantum tunneling conduction of completely separated PPy and CMC and tortuous conduction in a fully dispersed composite. The most likely arrangement exhibits thus a CMC-rich surface on PPy-rich nanospheres. In this scenario, the PPy concentration near the surface is drastically reduced, and the conductivity of the particle surface is low.

To test this hypothesis, depth profiling by SIMS was applied to the composite material. SIMS spectra show fragments of PPy, containing C, H, and N (dominantly CN^- and C_3N^-) as well as fragments of CMC, containing C, H, and O (C_2HO^-, CO_2H^-, $C_2H_3O_2^-$, and others). Depth profiling shows a CMC-rich surface (Figure 5a). The PPy concentration increases from the material surface to a constant value as the signal is averaged over multiple particles at different depths of ion milling. Electron energy loss spectroscopy (EELS) applied to the materials reveals that the PPy-rich nanospheres include a homogeneous distribution of CMC within the particles as a co-dopant. In contrast, a CMC surface layer is inhomogeneously distributed over the particle surface. This nanostructure is likely a consequence of the more hydrophilic nature of CMC compared to PPy. Acting as a surfactant, CMC thus coats the surface of PPy particles. Concurrently, CMC interacts with PPy as a co-dopant during polymerization and doping of PPy, leading to partial mixing of the two polymers. Notwithstanding the inhomogeneous CMC surface distribution, EELS analysis shows that CMC is enriched all over the PPy:CMC particle surface. The conductivity measurements demonstrate that the CMC-rich low-conductivity surface disrupts Ohmic conduction within the PPy:CMC composite.

CONCLUSIONS

The reported work shows that conducting polymer−polyanion composites can allow simple aqueous processing of plain conducting polymers for applications in which their electronic conduction is used. It demonstrates the formation of spherical nanostructures in PPy:CMC composites that are contained within a CMC matrix with significant impediment to their conduction behavior. The demonstrated pressure dependence of PPy:CMC electronic conductivity can be exploited for pressure sensors. While the presented material exhibits a pressure sensitivity that is several orders of magnitude smaller than those of metal-containing QTCs, design of the PPy particle shape has the potential to improve the performance of all-polymer QTCs. The composite needs further optimization for application of this principle in commercial pressure sensors. This includes an optimized PPy-to-CMC ratio for a targeted sensing range: a designed non-conductive polymer formulation, which can improve the elasticity of the non-conductive component; and processing parameters for targeted film thicknesses, robustness, optimized contact, and sensitivity. Moreover, with the design opportunities afforded by the use of conducting polymers, similar composites may be able to combine piezoresistive behavior with other properties, such as electroluminescence, for novel, pressure-sensitive electronics.

METHODS

PPy:CMC composites were synthesized *via* chemical oxidative *in situ* polymerization as described in the previous study.[13] Briefly, aqueous mixtures of pyrrole and Na−CMC were polymerized with $FeCl_3$ as oxidizing and polymerizing agents for 4 h in an ice bath. After immersing in ethanol solution overnight, PPy:CMC suspensions were filtered, washed with ethanol, and then dried at 80 °C under dynamic vacuum.

The morphologies of PPy:CMC composites were investigated by TEM (FEI Talos F200X microscope) and SEM (FEI Nova NanoSEM 450 microscope). X-ray photoelectron spectra were collected on a Kratos Axis Ultra X-ray photoelectron spectrometer with an aluminum anode. EELS and HAADF-TEM images were obtained at the Canadian Centre for Electron Microscopy on a FEI Talos 200X. The electrical conductivity of PPy:CMC composites with different PPy:CMC mass ratios was measured by the four-point probe method (Miller Design FPP-5000 instrument) on 0.6 mm-thick PPy:CMC pellets compressed at 200 MPa.

FTIR-ATR data were obtained with an Agilent Cary 670 spectrometer and a 620 IR imaging microscope with a slide-on

https://doi.org/10.1021/acsomega.2c03461
ACS Omega 2022, 7, 41937−41942

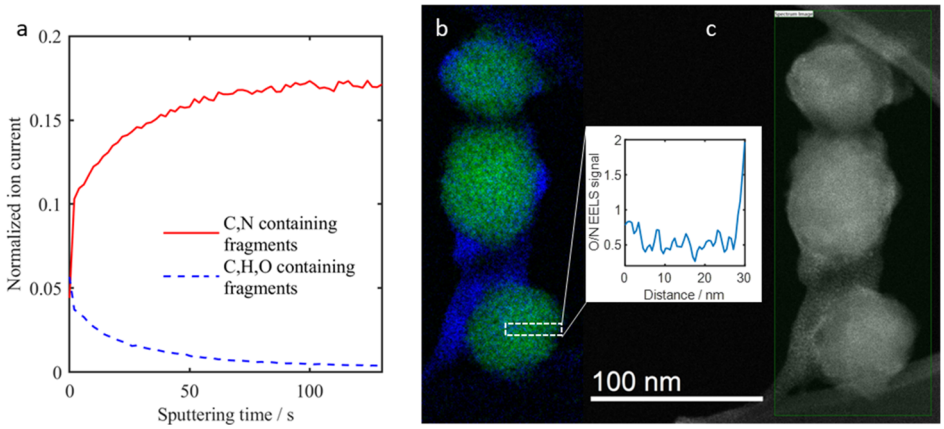

Figure 5. (a) SIMS depth profile showing the sum of CN^-, C_3N^- fragments (red solid line) and the sum of C_2HO^-, CO_2H^-, and $C_2H_2O_2^-$ fragments (blue dashed line). Additional fragments for each group were observed and behaved similarly to the presented data. (b) EELS map showing distribution of nitrogen (green) and oxygen (blue) as indicators of the presence of PPy and CMC, respectively, and (c) HAADF-TEM image with the EELS-mapped region highlighted. The inset shows a profile plot of the oxygen-to-nitrogen EELS signal ratio along the dashed rectangle.

Ge micro-ATR accessory. The micro-ATR contact area was imaged onto a 64 × 64 focal plane array detector, affording 4096 spectra per contact, with a nominal pixel resolution of 1.4 × 1.4 μm^2.[36] The material was dispersed on a glass slide, and at least three ATR contact images were obtained for each compound. The spectra were collected as a sum of 256 scans ratioed against an air background of 512 scans recorded at 4 cm^{-1} spectral resolution.

Pressure−response electrical conductivity measurements were performed on Au/Pd-coated PPy:CMC pellets by potentiostatic electrochemical impedance spectroscopy (EIS). PPy:CMC composites (50 mg) were ground and compressed at 25 MPa to form 0.3 mm-thick, 13 mm diameter PPy:CMC pellets. Pellets were sputter-coated with 15−20 nm-thick Au/Pd on both sides to eliminate contact resistance during measurement. Any coating along the edges that would allow a short circuit between the two sides was removed by carefully polishing the coated pellet. Au/Pd-coated PPy:CMC pellets were placed between two 13 mm diameter, T-shaped stainless steel rods covered by an insulating sample holder. The EIS measurement was performed using a potentiostat (Gamry Interface 1000E) running from 1 MHz to 0.1 kHz at different pressures. The pressure varied from 0 to 400 kPa by applying the appropriate weight to the sample die.

AUTHOR INFORMATION

Corresponding Author

Christian Kuss − *Department of Chemistry, University of Manitoba, Winnipeg R3T 2N2, Canada;* orcid.org/0000-0002-8598-5501; Phone: +1 (204) 480-1823; Email: christian.kuss@umanitoba.ca

Authors

Van At Nguyen − *Department of Chemistry, University of Manitoba, Winnipeg R3T 2N2, Canada*

Mariam Odetallah − *Department of Chemistry, University of Manitoba, Winnipeg R3T 2N2, Canada*

Gorkem Bakir − *Department of Chemistry, University of Manitoba, Winnipeg R3T 2N2, Canada;* orcid.org/0000-0002-1998-2927

Kathleen Gough − *Department of Chemistry, University of Manitoba, Winnipeg R3T 2N2, Canada*

Complete contact information is available at: https://pubs.acs.org/10.1021/acsomega.2c03461

Notes

The authors declare the following competing financial interest(s): A patent application, describing the use of these composites as piezoresistive devices, has been submitted.

ACKNOWLEDGMENTS

We gratefully acknowledge the financial support for this work from the Natural Sciences and Engineering Research Council Canada Discovery Grant program (C.K.: RGPIN-2019-05386 and K.G.: RGPIN/5931-2017), the University of Manitoba Graduate Fellowship program (V.A.N.), and the University of Manitoba Graduate Enhancement of Tri-council Stipend program (M.O. and G.B.). We also thank Benoit Girouard for technical assistance in the preparation of FTIR data, as well as Dr. Abdul Khan at the Manitoba Institute for Materials and Dr. Natalie Hamada at the Canadian Centre for Electron Microscopy for their assistance in collecting TEM data.

REFERENCES

(1) Skotheim, T. A.; Reynolds, J. R.*Handbook of Conducting Polymers*, 3rd ed.; CRC Press: Boca Raton, 2007.

(2) Wang, M.; Baek, P.; Akbarinejad, A.; Barker, D.; Travas-Sejdic, J. Conjugated Polymers and Composites for Stretchable Organic Electronics. *J. Mater. Chem. C* **2019**, *7*, 5534−5552.

(3) Khokhar, D.; Jadoun, S.; Arif, R.; Jabin, S. Functionalization of Conducting Polymers and Their Applications in Optoelectronics. *Polym. Technol. Mater.* **2021**, *60*, 465−487.

(4) Lu, B.; Yuk, H.; Lin, S.; Jian, N.; Qu, K.; Xu, J.; Zhao, X. Pure PEDOT:PSS Hydrogels. *Nat. Commun.* **2019**, *10*, 1043.

(5) Reza, K. M.; Gurung, A.; Bahrami, B.; Mabrouk, S.; Elbohy, H.; Pathak, R.; Chen, K.; Chowdhury, A. H.; Rahman, M. T.; Letourneau, S.; et al. Tailored PEDOT:PSS Hole Transport Layer for Higher Performance in Perovskite Solar Cells: Enhancement of Electrical and Optical Properties with Improved Morphology. *J. Energy Chem.* **2020**, *44*, 41−50.

(6) Sun, K.; Zhang, S.; Li, P.; Xia, Y.; Zhang, X.; Du, D.; Isikgor, F. H.; Ouyang, J. Review on Application of PEDOTs and PEDOT:PSS in Energy Conversion and Storage Devices. *J. Mater. Sci.: Mater. Electron.* **2015**, *26*, 4438−4462.

(7) Lepage, D.; Kuss, C.; Schougaard, S. B.Conducting Polymers in Lithium Batteries. In *Conducting Polymers: Synthesis, Properties and*

Applications; Almeida, L. C. P., Ed.; Nova Publishers, 2013; pp 291−314.
(8) Nguyen, V. A.; Kuss, C. Review—Conducting Polymer-Based Binders for Lithium-Ion Batteries and Beyond. *J. Electrochem. Soc.* **2020**, *167*, 065501.
(9) Guo, X.; Facchetti, A. The Journey of Conducting Polymers from Discovery to Application. *Nat. Mater.* **2020**, *19*, 922−928.
(10) Yang, Y.; Deng, H.; Fu, Q. Recent Progress on PEDOT:PSS Based Polymer Blends and Composites for Flexible Electronics and Thermoelectric Devices. *Mater. Chem. Front.* **2020**, *4*, 3130−3152.
(11) Xu, H.; Li, Y.; Jia, M.; Cui, L.; Chen, C.; Yang, Y.; Jin, X. Design and Synthesis of a 3D Flexible Film Electrode Based on a Sodium Carboxymethyl Cellulose−Polypyrrole@reduced Graphene Oxide Composite for Supercapacitors. *New J. Chem.* **2021**, *45*, 6630−6639.
(12) Xu, Y.; Zhang, Y. Synthesis of Polypyrrole/Sodium Carboxymethyl Cellulose Nanospheres with Enhanced Supercapacitor Performance. *Mater. Lett.* **2015**, *139*, 145−148.
(13) Nguyen, V. A.; Wang, J.; Kuss, C. Conducting Polymer Composites as Water-Dispersible Electrode Matrices for Li-Ion Batteries: Synthesis and Characterization. *J. Power Sources Adv.* **2020**, *6*, 100033.
(14) Wang, Y.; Zhu, L.; An, L. Electricity Generation and Storage in Microbial Fuel Cells with Porous Polypyrrole-Base Composite Modified Carbon Brush Anodes. *Renewable Energy* **2020**, *162*, 2220−2226.
(15) Wang, Y.; Wen, Q.; Chen, Y.; Li, W. Conductive Polypyrrole-Carboxymethyl Cellulose-Titanium Nitride/Carbon Brush Hydrogels as Bioanodes for Enhanced Energy Output in Microbial Fuel Cells. *Energy* **2020**, *204*, 117942.
(16) Wang, X.; Li, X.; Zhao, L.; Li, M.; Li, Y.; Yang, W.; Ren, J. Polypyrrole-Doped Conductive Self-Healing Multifunctional Composite Hydrogels with a Dual Crosslinked Network. *Soft Matter* **2021**, *17*, 8363−8372.
(17) Zou, Y.; Zhao, J.; Zhu, J.; Guo, X.; Chen, P.; Duan, G.; Liu, X.; Li, Y. A Mussel-Inspired Polydopamine-Filled Cellulose Aerogel for Solar-Enabled Water Remediation. *ACS Appl. Mater. Interfaces* **2021**, *13*, 7617−7624.
(18) Deeksha, B.; Sadanand, V.; Hariram, N.; Rajulu, A. V. Preparation and Properties of Cellulose Nanocomposite Fabrics with in Situ Generated Silver Nanoparticles by Bioreduction Method. *J. Bioresour. Bioprod.* **2021**, *6*, 75−81.
(19) Fatima, A.; Yasir, S.; Khan, M. S.; Manan, S.; Ullah, M. W.; Ul-Islam, M. Plant Extract-Loaded Bacterial Cellulose Composite Membrane for Potential Biomedical Applications. *J. Bioresour. Bioprod.* **2021**, *6*, 26−32.
(20) Chai, M. N.; Isa, M. I. N. Novel Proton Conducting Solid Bio-Polymer Electrolytes Based on Carboxymethyl Cellulose Doped with Oleic Acid and Plasticized with Glycerol. *Sci. Rep.* **2016**, *6*, 27328.
(21) Samsudin, A. S.; Khairul, W. M.; Isa, M. I. N. Characterization on the Potential of Carboxy Methylcellulose for Application as Proton Conducting Biopolymer Electrolytes. *J. Non-Cryst. Solids* **2012**, *358*, 1104−1112.
(22) Sasso, C.; Beneventi, D.; Zeno, E.; Chaussy, D.; Petit-Conil, M.; Belgacem, N. Polypyrrole and Polypyrrole/Wood-Derived Materials Conducting Composites: A Review. *BioResources* **2011**, *6*, 3585−3620.
(23) Lang, U.; Müller, E.; Naujoks, N.; Dual, J. Microscopical Investigations of PEDOT:PSS Thin Films. *Adv. Funct. Mater.* **2009**, *19*, 1215−1220.
(24) Horii, T.; Hikawa, H.; Katsunuma, M.; Okuzaki, H. Synthesis of Highly Conductive PEDOT:PSS and Correlation with Hierarchical Structure. *Polymer* **2018**, *140*, 33−38.
(25) Sasso, C.; Fenoll, M.; Stephan, O.; Beneventi, D. Use of Wood Derivatives as Doping/Dispersing Agents in the Preparation of Polypyrrole Aqueous Dispersions. *BioResources* **2008**, *3*, 1187−1195.
(26) Koh, D.; Foulds, I. S.; Aw, T. C. Dermatological Hazards in the Electronics Industry. *Contact Dermatitis* **1990**, *22*, 1−7.
(27) Calvert, P.; Patra, P.; Lo, T.-C.; Chen, C. H.; Sawhney, A.; Agrawal, A.Piezoresistive Sensors for Smart Textiles. *Proceedings SPIE 6524, Electroactive Polymer Actuators and Devices (EAPAD)*, 2007; p 65241I.
(28) Tjaden, B.; Cooper, S. J.; Brett, D. J. L.; Kramer, D.; Shearing, P. R. On the Origin and Application of the Bruggeman Correlation for Analysing Transport Phenomena in Electrochemical Systems. *Curr. Opin. Chem. Eng.* **2016**, *12*, 44−51.
(29) La Rue, R. E. D.; Tobias, C. W. On the Conductivity of Dispersions. *J. Electrochem. Soc.* **1959**, *106*, 827.
(30) Chung, D.-W.; Ebner, M.; Ely, D. R.; Wood, V.; Edwin García, R. Validity of the Bruggeman Relation for Porous Electrodes. *Modell. Simul. Mater. Sci. Eng.* **2013**, *21*, 074009.
(31) Ding, S.; Han, B.; Dong, X.; Yu, X.; Ni, Y.; Zheng, Q.; Ou, J. Pressure-Sensitive Behaviors, Mechanisms and Model of Field Assisted Quantum Tunneling Composites. *Polymer* **2017**, *113*, 105−118.
(32) Cartlidge, E. Entrepreneur Exploits Quantum Physics. *Phys. World* **2003**, *16*, 8.
(33) Stassi, S.; Sacco, A.; Canavese, G. Impedance Spectroscopy Analysis of the Tunnelling Conduction Mechanism in Piezoresistive Composites. *J. Phys. D: Appl. Phys.* **2014**, *47*, 345306.
(34) Granger, R. M.; Yochum, H. M.; Granger, J. N.; Sienerth, K. D.Scanning Tunneling Microscopy. In *Instrumental Analysis*; Oxford University Press, 2017; pp 711−714.
(35) Inganäs, O.; Skotheim, T.; Lundström, I. Polypyrrole-semiconductor Schottky Barriers. *J. Appl. Phys.* **1983**, *54*, 3636−3639.
(36) Findlay, C. R.; Wiens, R.; Rak, M.; Sedlmair, J.; Hirschmugl, C. J.; Morrison, J.; Mundy, C. J.; Kansiz, M.; Gough, K. M. Rapid Biodiagnostic Ex Vivo Imaging at 1 Mm Pixel Resolution with Thermal Source FTIR FPA. *Analyst* **2015**, *140*, 2493−2503.

https://doi.org/10.1021/acsomega.2c03461
ACS Omega 2022, 7, 41937−41942